DFT study on binding of single and double methane with aromatic hydrocarbons and graphene: stabilizing CH···HC interactions between two methane molecules

Jovian Lazare, Dalia Daggag & Tandabany Dinadayalane

Structural Chemistry
Computational and Experimental Studies of Chemical and Biological Systems

ISSN 1040-0400
Volume 32
Number 2

Struct Chem (2021) 32:591-605
DOI 10.1007/s11224-020-01657-y

Structural Chemistry (2021) 32:591–605
https://doi.org/10.1007/s11224-020-01657-y

ORIGINAL RESEARCH

DFT study on binding of single and double methane with aromatic hydrocarbons and graphene: stabilizing CH···HC interactions between two methane molecules

Jovian Lazare[1] · Dalia Daggag[1] · Tandabany Dinadayalane[1]

Received: 7 July 2020 / Accepted: 30 September 2020 / Published online: 20 October 2020

Abstract

Density functional theory (DFT) calculations were used to examine the binding strength of one and two methane molecule(s) with graphene (62 and 186 carbon atoms) and model systems of aromatic hydrocarbons (benzene, pyrene, and coronene). We explored different possibilities of binding modes of methane such as one, two, and three C-H interacting with small π-systems. Two methane molecules were considered to bind from the same as well as opposite sides of the plane of benzene and other π-systems including graphene models. Our results show that methane molecule prefers to bind with three C-H···π interactions with all the π-systems except benzene. The preference of tripod configuration of methane on the surface of graphene systems strongly agrees with the neutron diffraction experiment of methane on graphitized carbon black. The binding strength is almost doubled by increasing the number of methane molecules from one to two. Importantly, two methane molecules prefer to bind on the same side rather than opposite sides of the plane of graphene due to stabilizing CH···HC interactions between them in addition to six C-H···π interactions. Interestingly, binding strength contributions from CH···HC interactions (approx. 0.4–0.5 kcal/mol) of two methane molecules on the surface are analogous to methane dimer complex free from the surface of graphene. C-H stretching frequency shifts, bond lengths, and binding distances support the presence of CH···HC interactions between two methane molecules. Structures of complexes, binding energies, and C-H stretching frequency shifts agree with available experimental data.

Keywords Density functional theory · HOMO-LUMO energy gap · Graphene · Methane storage · Molecular sensors · CH···π interactions · CH···HC interactions

Introduction

Growing demand of natural gas resources has led to interests in unconventional gas sources such as shale, tight gas, and methane hydrates [1–5]. Methane (CH_4) is a high-energy molecule with the highest hydrogen to carbon ratio compared to other hydrocarbons. Thus, it is a low-pollution energy source [6–8]. Methane is the primary source of natural gases, biogas, and landfill gas [9–12]. When technical difficulties of accessing methane from methane hydrates are addressed, there will be enormous potential for CH_4 reserves around the world [5]. Exploration of different materials is crucial to identify light-weight, efficient, cost-effective, safe, and high surface area materials for methane storage. Recently, adsorption of natural gas including methane on the graphene sheets have been studied experimentally [13, 14]. Graphene oxide was reported as an optimal candidate for methane storage [15]. Mahmoudian et al. proposed a new and economical synthetic pathway for the mass production of graphene of ~ 3000 m^2/g specific surface area that will be suitable to achieve desirable efficacy in methane uptake/storage [16].

Release of methane into the environment accelerates global warming because it is a potent heat trap and its impact on climate change can be greater than carbon dioxide [6, 9]. Owing to the danger from possible leakages of methane, the development of reliable and low-cost methane sensors is important [9, 17, 18]. Some progress has been made over the

Electronic supplementary material The online version of this article (https://doi.org/10.1007/s11224-020-01657-y) contains supplementary material, which is available to authorized users.

✉ Tandabany Dinadayalane
dtandabany@cau.edu

[1] Department of Chemistry, Clark Atlanta University, 223 James P. Brawley Drive, S.W, Atlanta, GA 30314, USA

years in methane sensor development. However, current methane sensors are bulky, expensive, and require too many variables or prone to contamination. Computational study of Yang et al. revealed that stacked graphene sheets substantially increase adsorption strength with methane molecule implying improved sensor performance [19]. Graphene-based materials produced by surface modification (doping or functionalization) are useful for gas sorption, storage, and separation [20–23]. It should be highlighted that graphene-based materials are expected to be suitable for sensors due to light-weight and tunability [24, 25]. Nitrogen-doped graphene systems have showed the potential to serve as sensors [26]. Wu et al. produced methane sensors that work at room temperature by using graphene nanosheets/polyaniline composites [27].

A thorough understanding of structural and electronic properties of molecular interactions involving small molecules and graphene-based systems is required to enable the design and optimization of new nanodevices. Computational methods provide valuable insight into the properties of molecular systems/complexes and often complement experimental research in many areas of chemistry, nanoscience, and nanotechnology [28–30]. Numerous contributions have been made in the modeling of a single methane molecule with benzene and polycyclic aromatic hydrocarbons (PAHs) that include pyrene and coronene [29, 31–39]. Tsuzuki et al. showed that the C-H bond of methane prefers to stabilize over the benzene ring primarily due to dispersion interaction [29]. In further work, mass analyzed threshold ionization spectroscopy was used to study the methane-benzene cluster in the gas phase [32]. Sherrill and co-workers investigated methane-benzene, methane-phenol, and methane-indole complexes that are prototypes for C-H interactions with aromatic rings of amino acids of phenylalanine, tyrosine, and tryptophan [31]. C-H···π interactions involving naturally occurring α-amino acids with graphene and graphene oxide have been studied both computationally and experimentally [40–45]. Such investigations including model or prototype systems are useful to enhance our understanding of protein environments, drug design, materials design, and supramolecular chemistry. DFT calculations predicted the existence of weak scalar (*J*) couplings between nuclei involved in methyl/π interactions in proteins. It should be noted that experimental nuclear magnetic resonance (NMR) spectroscopy has been used to directly detect the C-H···π (methyl/π) interactions in proteins at atomic resolution and confirmed the predicted *J* couplings [46].

Finite PAHs such as coronene ($C_{24}H_{12}$), hexabenzocoronene ($C_{42}H_{18}$), circumcoronene ($C_{54}H_{18}$), and circumcircumcoronene ($C_{96}H_{24}$) were used as non-periodic models of graphene to study with small molecule interactions [28, 35, 47–52]. Experimental values of isosteric heats of adsorption for methane binding with graphite in gas phase were reported [53–55] and those values were generally used to compare the computational results relevant to the interactions of single methane with abovementioned non-periodic models of graphene [35, 37]. To the best of our knowledge, the studies on binding of two methane molecules with graphene models are not available.

In this study, quantum chemical calculations at the DFT level were used to examine the structures and binding affinities of one and two methane interactions with aromatic hydrocarbons (benzene (**B**), pyrene (**P**), and coronene (**C**)) and two finite size graphene models (small graphene (**G1**) and large graphene (**G2**) containing 62 and 186 carbon atoms, respectively) (Scheme 1). The edges of graphene sheets were terminated by hydrogen atoms. This study is aimed to (a) assess the C-H···π interactions of methane with graphene and compare the results obtained for small π-systems of benzene, pyrene, and coronene; (b) predict the selectivity of same or opposite side for two methane interactions with considered polycyclic π-systems; and (c) report and discuss the C-H vibrational frequency shifts of methane in the complexes with respect to C-H of free methane molecule in order to support future experiments to confirm the formation of complexes.

Computational details

All calculations were carried out using NWCHEM 6.6 program package [56]. Geometry optimizations of monomers and complexes were performed using M06-2X functional in conjunction with 6-31G(d) basis set imposing symmetry restrictions when available [57]. The option of the finest grid was chosen in performing calculations. The meta-hybrid density functional M06-2X provides reliable results at affordable computational cost for non-bonding interactions of π-π and C-H···π interactions [57, 58]. The binding energies were corrected for the basis set superposition error (BSSE) using counterpoise technique proposed by Boys and Bernardi [59]. The following equations were used to calculate the binding energies:

$$\Delta E_b = -[E(\text{complex}) - E(\pi\text{–system}) - nE(CH_4)] \quad (1)$$

$$\Delta E_b{}^{CP} = \Delta E_b - E_{BSSE}{}^{CP} \quad (2)$$

where ΔE_b denotes binding energy; E(complex) denotes the energy of the complex formed after geometry optimization; E(π-system) denotes the energy of the π-system considered here; n indicates the number of methane molecules, $n = 1$ or 2; $\Delta E_b{}^{CP}$ denotes the binding energy with BSSE correction. $E_{BSSE}{}^{CP}$ denotes the BSSE correction value obtained from the counterpoise calculation.

Unlike the small complexes, it was not possible to calculate the BSSE correction in straightforward single calculation for the large graphene system using NWCHEM. Therefore, we have calculated the BSSE-corrected binding energies using

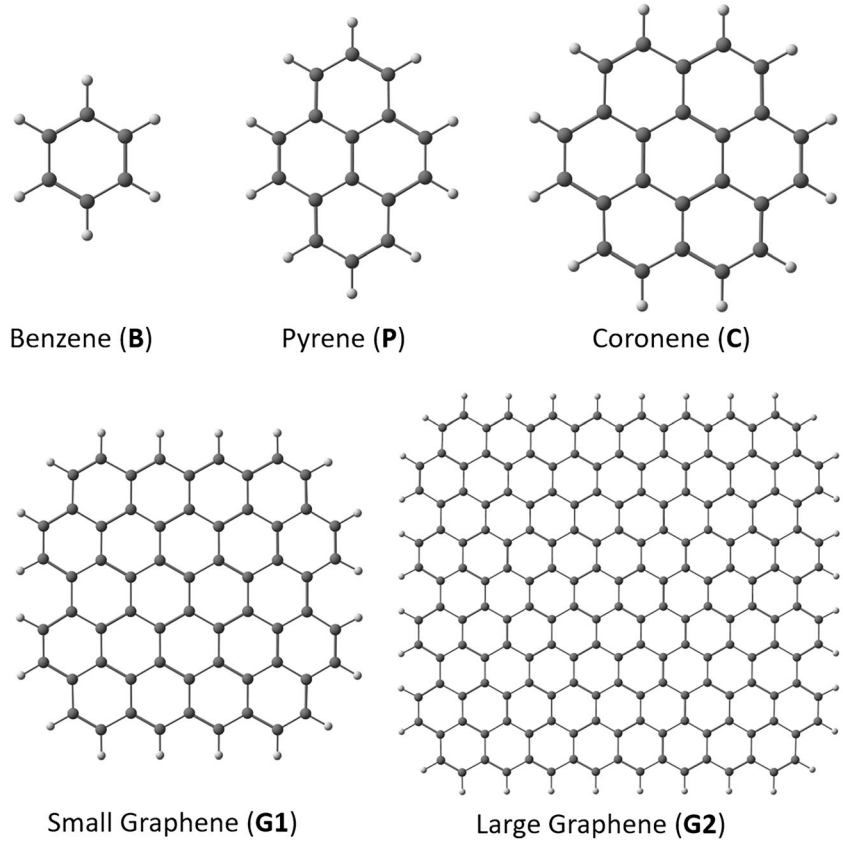

Scheme 1 Structures of benzene and polycyclic π-systems

the following equations:

$$\Delta E_b^{CP} = \Delta E_b - [E_A - E_A^{AB}] - [E_B - E_B^{AB}] \quad (3)$$

$$\Delta E_b^{CP} = \Delta E_b - [E_A - E_A^{ABC}] - [E_B - E_B^{ABC}] - [E_C - E_C^{ABC}] \quad (4)$$

where A, B, and C represent monomers of the respective complex. "A" denotes the aromatic system, "B" denotes the first methane molecule, and "C" denotes the second methane molecule. E_A, E_B, and E_C denote the energies of monomer separated from the respective complex. E_A^{AB} and E_B^{AB} denote the energy of monomer A in dimer basis and the energy of monomer B in dimer basis, respectively. E_A^{ABC} denotes the energy of monomer A in trimer basis. Thus, the functions on B and C are "ghost functions," or the atoms of B and C are treated as "ghost atoms" in a computation for E_A^{ABC}. A similar approach was used for computation of E_B^{ABC} and E_C^{ABC}.

All binding energies are reported along with BSSE corrections in kcal/mol. M06-2X/6-31G(d) level optimized geometries were used to obtain the highest occupied molecular orbital (HOMO) and the lowest unoccupied molecular orbital (LUMO) energies and their energy gaps at the TPSSh/6-31G(d) level [60, 61]. Previous studies reported that TPSSh functional is reliable to produce HOMO-LUMO energy gaps including for carbon-based nanomaterials [62–66]. Frequency calculations were performed at M06-2X/6-31G(d) level for individual fragments and selected complexes to examine C-H stretching frequencies and intensities. The recommended scaling factor of 0.947 was applied for all vibrational frequencies [67]. Our current computational resources do not allow us to perform expensive frequency calculations for large graphene and its complexes.

Results and discussion

In this representative study, we have explored one hydrogen (1H), two hydrogens (2H), and three hydrogens (3H) of methane molecule interacting with π-systems of benzene (**B**), pyrene (**P**), and coronene (**C**). When the complexes were built for 1H of methane interacting with the abovementioned π-systems, we considered placing the interacting hydrogen of CH_4 above the center of the ring, above the center of C-C bond, and above different carbon atoms of π-systems. Based on the data obtained from these calculations, the interactions involving 3H of methane were considered for graphene systems. Notably, our putative complexes with 1H of methane binding with small graphene were collapsed to complexes having 3H interactions. Several complexes were obtained after detailed exploration. Only thirty-six (36) of the most stable complexes as well as selected complexes having high binding energy are provided here for all five π-systems (**B**, **P**, **C**, **G1**, and **G2**). However, all remaining complexes obtained are

given in the supplementary information. For naming of the complexes, the letters **B**, **P**, **C**, **G1**, and **G2** are used to indicate the π-systems, and the letters of lowercase **s** and **d** correspondingly indicate single and double methane. For example, **B-s-1** means the first complex of benzene with single methane.

Equilibrium geometries of the complexes

The structures obtained at the M06-2X/6-31G(d) level for methane and its dimer are shown in Fig. 1. The C-H bond length is 1.091 Å for methane and the same value is retained for C-H bond in the methane complex. The non-bonding intermolecular H···H distance in methane dimer is 2.94 Å. The complexes of single and double methane binding with **B**, **P**, and **C** are displayed in Fig. 2. C-H bond lengths of methane and non-bonding distances in the complexes are shown. As mentioned in the previous studies [36, 39], the structure possessing only plane of symmetry for the complex in which 1H interacting with **B** is more stable (by 0.17 kcal/mol) than the structure having C_{3v} point group. The intermolecular distance between H (of CH_4) and the center of π-ring is either 2.67 or 2.68 Å for the complexes, **B-s-1**, **B-d-1**, and **B-d-2**, which all possess a bent orientation of methane. However, the intermolecular distance reduces to 2.55 Å for the complex of **B-d-3** that possesses a straight orientation of methane with higher order of symmetry (D_{3h}).

In contrast to methane-benzene complexes, the most stable complexes for methane-pyrene and methane-coronene exhibit 3H interacting with the π-system (Fig. 2). This trend persists when we increase the number of methane from one to two in forming the complexes. Previous studies reported the same observation for complexes involving **P** and **C** with single methane [33, 35, 38]. As mentioned earlier, studies concerning binding of two methane molecules with polycyclic π-systems including graphene were not yet reported. Selectivity of same or opposite side of the π-systems for binding of two methane molecules is an important aim of this paper.

Figure 3 shows the structures of the complexes of methane binding with small graphene depicting selected distances.

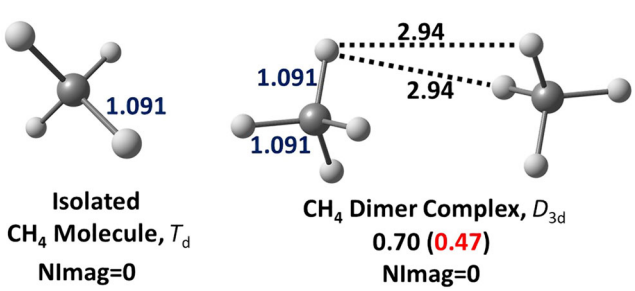

Fig. 1 M06-2X/6-31G(d) level optimized geometries of free methane and its dimer complex are shown with their point groups and number of imaginary frequency (NImag). Binding energy (BSSE-corrected binding energy) values are provided for methane dimer

Figures 4 and 5 display the complexes of single and double methane binding with large graphene, respectively. 2H or 3H interactions of methane with **P**, **C**, **G1**, and **G2** produce longer C-H···π distances compared to methane-benzene complex. As shown in Figs. 2, 3, and 4, **P-s**, **C-s**, **G1-s**, and **G2-s** have C-H···π distances of 2.81–2.88 Å, 2.84–2.92 Å, 2.82–2.92 Å, and 2.81–2.93 Å, respectively. These ranges are not significantly changed while moving from pyrene to graphene complexes. Our results reveal the preference of tripod configuration of methane on the surface of polycyclic π-systems including graphene. This observation strongly agrees with the neutron diffraction experiment reporting the tripod configuration of methane on the surface of graphitized carbon black [68]. The reported experimental value of methane-carbon to surface carbon of graphitized carbon black distance is 3.35 ± 0.1 Å [68]. In agreement with this experimental value, our computational study yields the distances of 3.23 Å for methane-graphene complexes and the same value is retained for methane-coronene and methane-pyrene complexes.

The C-H···π distances in double methane complexes of **P-d**, **C-d**, **G1-d**, and **G2-d** are 2.76–2.90 Å, 2.74–2.91 Å, 2.79–2.95 Å, and 2.80–2.93 Å, respectively (Figs. 2, 3, and 5). The distances of ≤ 2.80 Å are observed for the complexes having two methane molecules that are on the same side of π-system as well as in close contact. The distribution of intermolecular H···H distances in crystal structures of tertiary alkanes retrieved from the Cambridge Structural Database (CSD) is in the range 2.1–3.0 Å and the majority of structures reported to have the distance of 2.72 Å [69]. At least one of the H···H distances between two methane molecules is 2.69 Å in the complexes of **P-d-2**, **C-d-2**, **G1-d-9**, and **G2-d-4**. In case of all four complexes, some H···H distances are about 2.7 Å whereas longer H···H distances of 3.4–3.7 Å are observed for latter two complexes. Non-bonding distances of CH···HC confirm the interactions between two methane molecules in addition to multiple C-H···π interactions in complexes of **P-d-2**, **C-d-2**, **G1-d-9**, and **G2-d-4**. For many of the complexes, the bond length of interacting C-H of methane (in C-H···π interactions) is 1.092 or 1.093 Å. The distance of C-H bond in bare methane is 1.091 Å. The interacting C-H bonds elongate insignificantly by 0.001 or 0.002 Å.

Binding energies and HOMO-LUMO energy gaps

Available experimental results of adsorption energies of methane binding with benzene, graphene, and graphite are listed in Table 1. BSSE-corrected binding energy for methane-benzene calculated at M06-2X/6-31G(d) level is 1.17 kcal/mol. This value indicates the stable complex and is comparable to the experimental dissociation energy of 1.03–1.13 kcal/mol in the gas phase (Tables 1 and 2) [32]. The BSSE correction is a significant quantity (0.75 kcal/mol) at M06-2X/6-31G(d) level for benzene-methane complex and inclusion of this

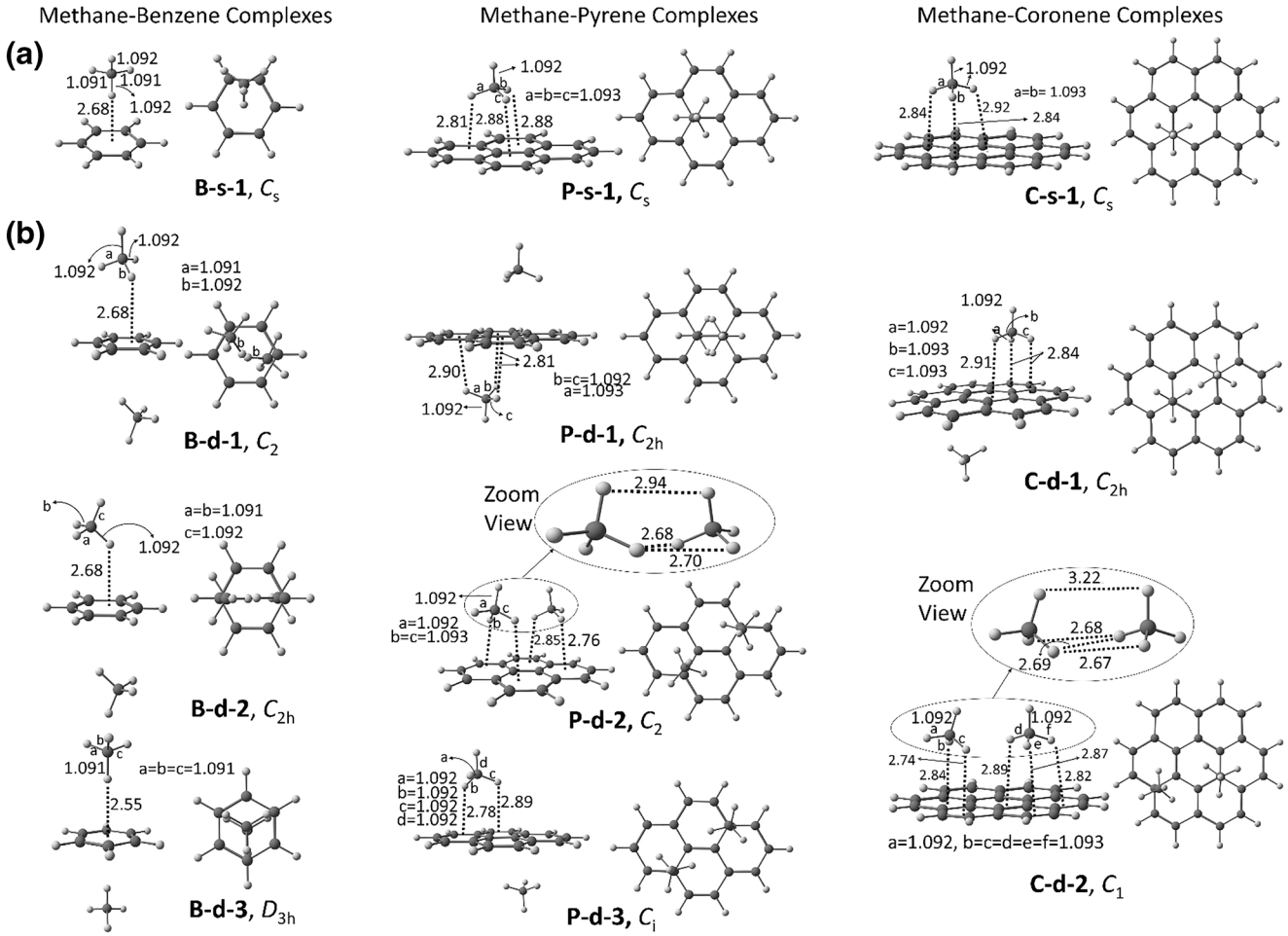

Fig. 2 C-H bond lengths of methane molecules and non-bonding CH···π distances obtained at the M06-2X/6-31G(d) level for selected complexes formed by **a** single methane and **b** double methane with benzene (**B**), pyrene (**P**), and coronene (**C**). CH···HC non-bonding distances are also provided for complexes involving double methane. Side and top views are given for each complex and all distances are in Å

correction is meaningful based on the above comparison. The BSSE corrections for other complexes are notable values. However, the binding energy trend is generally not changed with and without BSSE correction. It should be noted that the BSSE correction is expected to change as the functional and/or the basis set is changed. Interestingly, two different ranges of values were published for methane interactions with graphene (Table 1). The isosteric heat of adsorption for CH_4 on graphene sheets was reported to be 2.42 to 3.40 kcal/mol [13]. However, different studies by Zhu et al. revealed the corresponding values of 4.57 to 4.65 kcal/mol [14]. The first range of values are closer to the values provided in the literature for methane-graphite complexes (2.75–3.23 kcal/mol) [53]. These experimental reports strongly suggest that measurement of binding strength of methane or other hydrocarbons like ethane, propane, and butane with graphene or graphene oxide are possible in gas phase. As provided in Table 2, BSSE-corrected binding energy for methane-graphene (large) is 2.07–2.12 kcal/mol depending on the location of the methane on graphene surface. It should be noted that the computational data from quantum chemical calculations will stimulate further experimental research in exploring controlled methane adsorption with graphene.

In this study, several possibilities for the complexes were examined. For single methane binding, 12, 14, 19, and 16 complexes were obtained for benzene, pyrene, coronene, and small graphene, respectively. In case of double methane binding, 16, 29, 32, and 12 complexes were explored for the respective π-systems. Only selected complexes are given in the paper and all remaining complexes with their point groups and binding energies are provided in the supplementary information. Generally, the small change in orientation of methane binding on the π-system does not significantly affect the binding energy for all the π-systems considered. It should be noted that many isoenergetic complexes were found specifically in cases where one hydrogen atom of CH_4 interacts with benzene (see supplementary information, Figs. S1 and S2). This is analogous to the previous report disclosing of few isoenergetic complexes possessing single hydrogen of methane binding with benzene [29]. Several isoenergetic and nearly

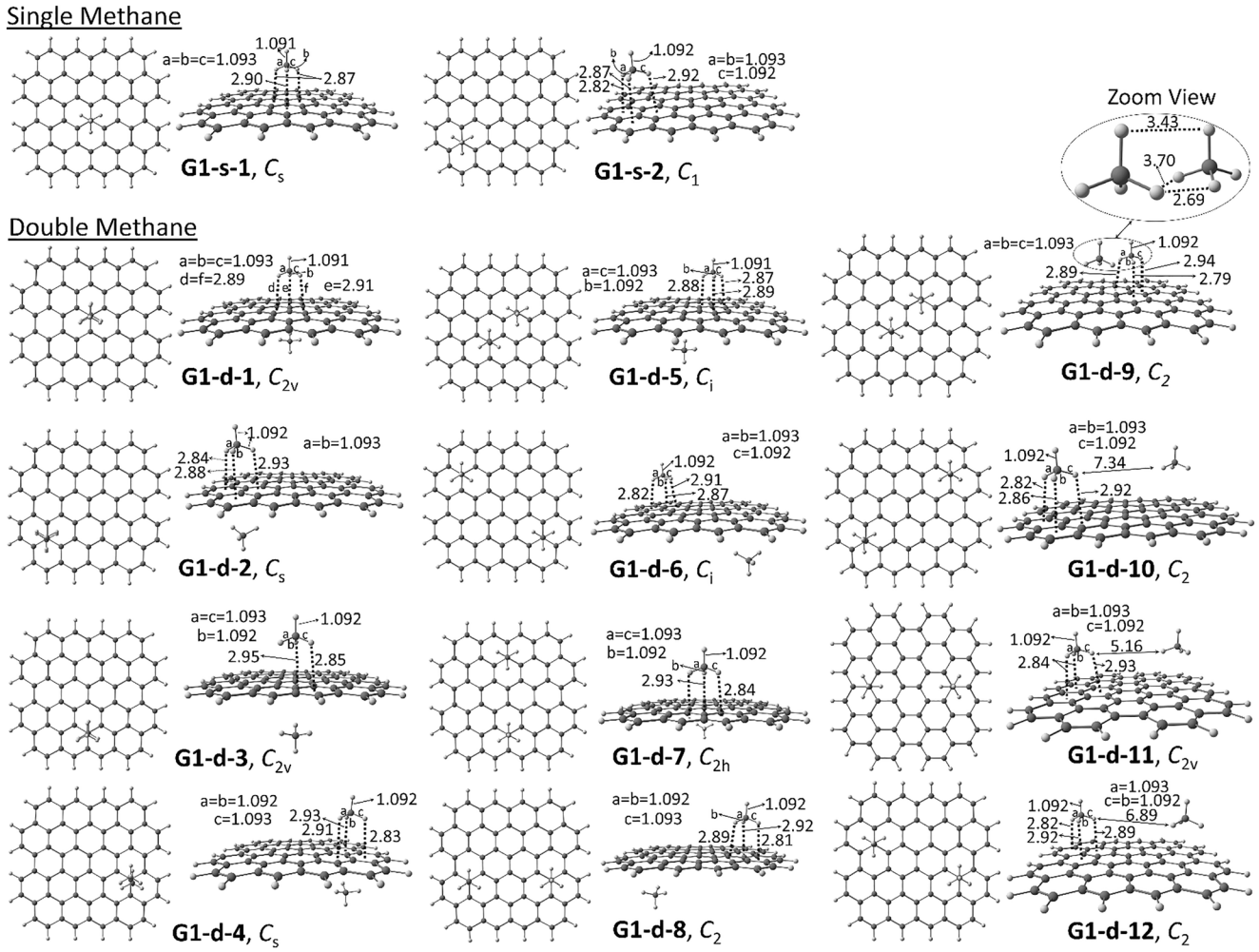

Fig. 3 C-H bond lengths of methane and non-bonding distances obtained for low-energy complexes of small graphene (**G1**)-single methane and small graphene (**G1**)-double methane (side and top views are shown). All distances are in Å

isoenergetic structures were obtained for the complexes involving pyrene, coronene, and graphene (see supplementary information, Figs. S3-S8).

After thorough examination, we found that the most stable complex (**B-s-1**) is the bent orientation of CH_4 with one C-H···π interaction above the center of benzene ring as reported by a previous study [36]. In case of double methane binding to benzene, the bent orientation is preferred over straight C-H interaction of methane (complex having a C_3 axis of rotation) on π-cloud as shown in Fig. 2 and Table 2. 1H interaction is more favorable than 2H and 3H interactions of methane with benzene (supplementary information, Figs. S1 and S2). Conversely, 3H interactions are more preferred than 1H interaction of methane with other π-systems (pyrene, coronene, and small graphene).

Table 2 and Fig. 6 show that the binding energy increases significantly when the number of methane molecules is increased from one to two. For single methane binding, pyrene shows slightly stronger binding affinity (approximately 0.2 kcal/mol) than coronene and graphene (binding energies are 2.07–2.12 kcal/mol). For the adsorptions of single methane, the binding energy is not altered significantly by changing the size of graphene from **G1** to **G2**. The same scenario was observed in case of two methane molecules binding with graphene models. Due to the availability of large surface area of graphene, two methane molecules can be placed in different locations. Although many different configurations were obtained for complexes involving graphene, the binding energy values are either too close or the same for numerous structures. Binding of two methane molecules with coronene and graphene provides interesting results. Figure 6 clearly indicates that two methane molecules prefer to be close to each other upon binding with graphene. This is due to stabilizing intermolecular CH···HC interactions between two methane molecules that establish the most stable orientation while having multiple CH···π interactions with graphene.

CH···HC interactions are still not well understood. It should be mentioned that H···H stabilizing interactions have been investigated recently by different groups [37, 69–71]. Experimental and computational studies labeled CH···HC

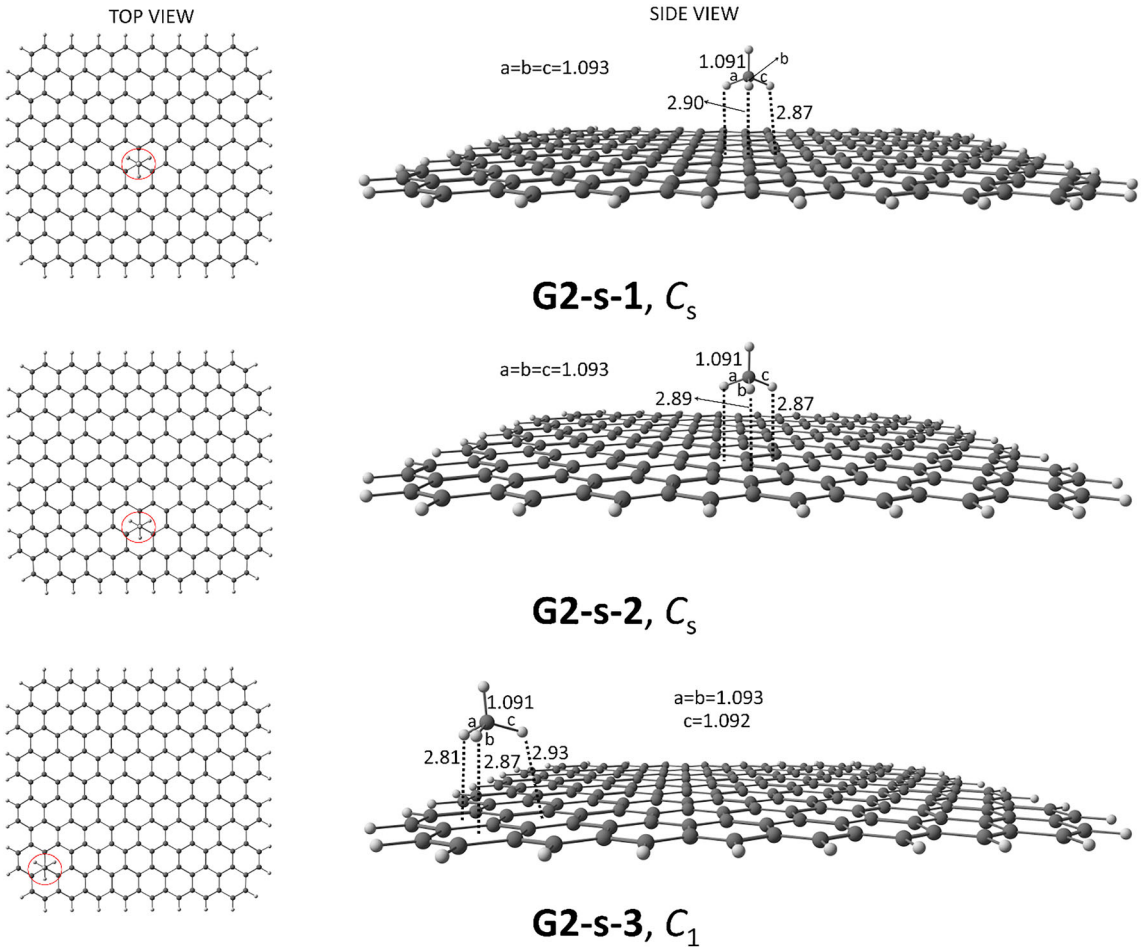

Fig. 4 C-H bond lengths of methane and CH···π non-bonding distances for selected complexes of large graphene (**G2**)-single methane (top and side views are shown). Location of methane on the surface of graphene in top view is highlighted by red circle. All distances are in Å

interactions as "sticky fingers" [72–75]. Rosel et al. reported the shortest intermolecular H···H distance of 1.566 Å using neutron diffraction experiments. Quantum chemical computations complement the experimental result of H···H distance in solid state (1.555 Å) and gas-phase (1.634 Å) for the dimer of tri(3,5-*tert*-butylphenyl)methane. Intermolecular London dispersion forces were reasoned for the stabilization of remarkably short H···H contacts [71]. Danovich et al. made an excellent attempt to reveal the true nature of the stability of intermolecular H···H interactions by using valence bond models and a perturbation approach to describe alternating charges that bring an electrostatic component to the stability of alkane dimers [69]. As given in Table 2, the highest binding energies of 4.35 (**C-d-2**), 4.61 (**G1-d-9**), and 4.64 (**G2-d-4**) kcal/mol were obtained for double methane complexation with **C**, **G1**, and **G2**, respectively. All three complexes possess intermolecular H···H interactions between two methane molecules in addition to C-H···π interactions with π-systems.

It is important to mention that binding energies are not noticeably changed when moving the location of single methane while maintaining the same orientation on the surface of graphene. This trend also continues for double methane binding with graphene except when two methane molecules are close to each other with the shortest intermolecular H···H distances (**G1-d-9** and **G2-d-4**). For the complexes in which two methane molecules are apart on same side of graphene, the closest H···H distance between two methane is 7.34, 5.16, and 6.89 Å (Fig. 3) for **G1-d-10**, **G1-d-11**, and **G1-d-12**, respectively. The corresponding binding energies are 4.20, 4.21, and 4.15 kcal/mol. In case of large graphene complexes, the abovementioned distance increased to 8.95, 10.43, and 20.35 Å (Fig. 5) for **G2-d-3** (4.12 kcal/mol), **G2-d-7** (4.13 kcal/mol), and **G2-d-8** (4.20 kcal/mol), respectively. Our study reveals that intermolecular interactions between two methane molecules have shown impact on binding energies while those molecules interact with graphene and coronene. Three pairs of complexes involving graphene yield practically the same binding energy values. Complex pairs (binding energies) are given here: **G1-d-6** and **G1-d-10** (4.20 kcal/mol); **G1-d-7** and **G1-d-11** (4.21 kcal/mol); **G2-d-5** and **G2-d-8** (4.20 kcal/mol). In the first pair of complexes, two methane molecules are on opposite sides of the plane in

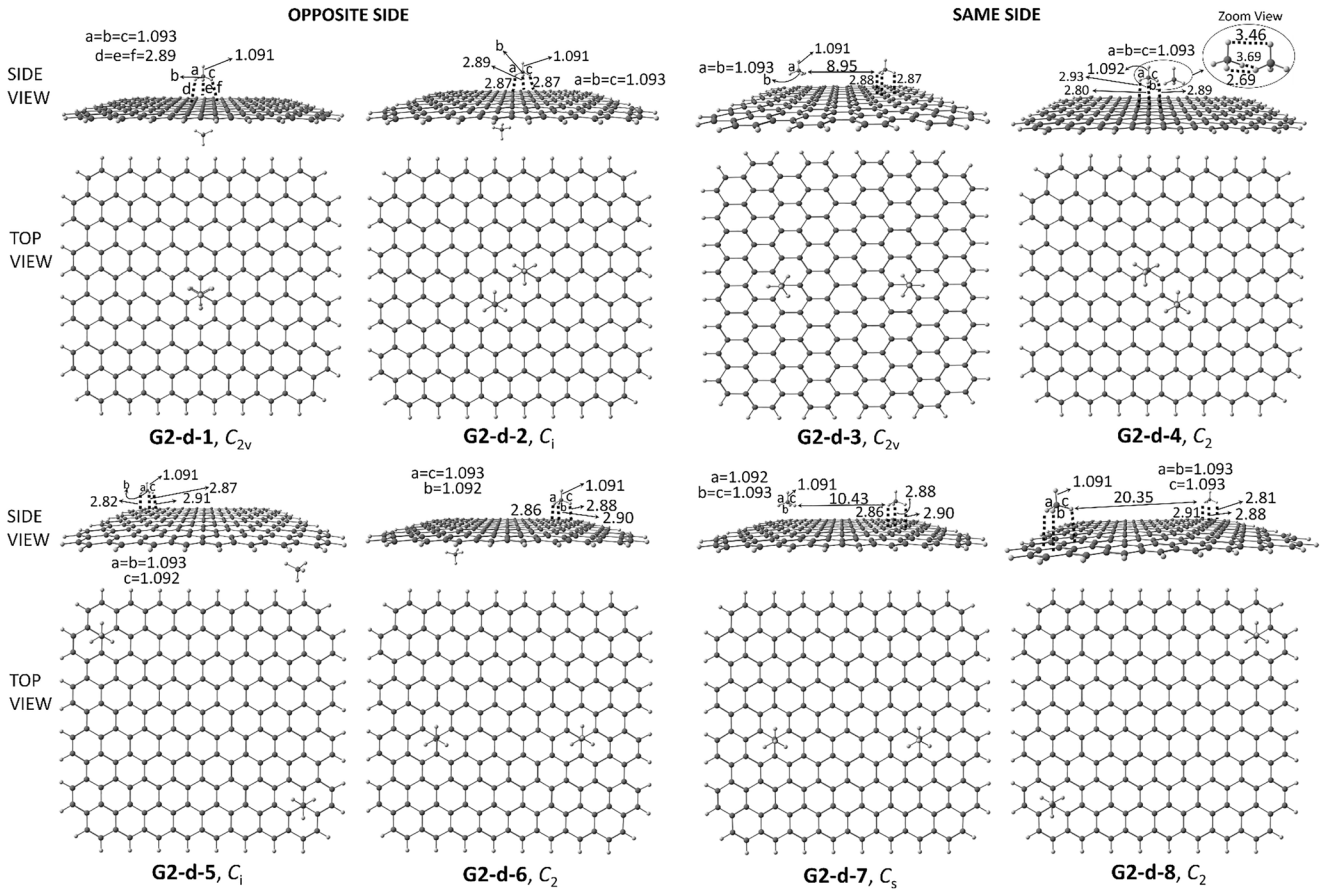

Fig. 5 C-H bond lengths of methane and non-bonding distances such as CH···π and CH···HC obtained for low-energy complexes of large graphene (**G2**)-double methane (side and top views are shown). All distances are in Å

G1-d-6 and they are on the same side in **G1-d-10**. The binding energies of these pairs indicate that the preference of same or opposite side is immaterial if two methane molecules do not interact with each other. Structures of the complexes and their binding energies reveal that the edge rings have negligible effect compared to the inner rings of graphene. Two methane molecules are aligned directly on opposite sides of graphene in the structures from **G1-d-1** to **G1-d-4** and **G2-d-1**. In these five complexes, two methane molecules share the same three six-membered rings for C-H···π interactions. The binding energies of these complexes are 4.09–4.25 kcal/mol, which are comparable to other configurations except **G1-d-9** and **G2-d-4** possessing intermolecular H···H interactions between two methane molecules.

Table 1 Available experimental results of adsorption energies (in kcal/mol) for methane binding with π-systems along with the references

π-System	Ads. E. (kcal/mol)	Ref.
Benzene	1.03–1.13[a]	[32]
Graphene	2.42–3.40[b]	[13]
Graphene	4.57–4.65[c]	[14]
Graphite	2.75–3.23[d]	[53]
Graphite	2.91[e]	[53]

[a] Mass analyzed threshold ionization (MATI) technique was used to report the dissociation energy

[b] Isosteric heat of adsorption was measured using Gibbs-Helmholtz equation and from the slope of the isosteric curves of adsorption

[c] Isosteric heat at zero surface loading was reported at temperature range 253.15–293.15 K using Henry's law

[d] Based on isosteric heat of adsorption and virial coefficient measurements

[e] Best estimate of ground state binding energy

P-d-1 complex exhibits six C-H···π interactions like the complexes of graphene listed in Table 2. Therefore, its binding energy (4.24 kcal/mol) is very close to the binding energies obtained for graphene complexes. Like **G1-d-9** and **G2-d-4**, the intermolecular stabilizing H···H interactions exist in case of **P-d-2** and **C-d-2**, and their respective binding energies are 3.94 and 4.35 kcal/mol. The lower binding energies for these complexes compared to **G1-d-9** and **G2-d-4** could be explained based on the number of C-H···π interactions. Because of the small size of the π-systems of coronene and pyrene, two methane molecules form only 5 and 4 intermolecular C-H···π interactions along with H···H interactions in **C-**

Table 2 Binding energies (ΔE_b), BSSE correction (E_{BSSE}^{CP}), and BSSE-corrected binding energies (ΔE_b^{CP}) for single and double methane in kcal/mol

System	Single methane				Double methane			
	Complex	ΔE_b	E_{BSSE}^{CP}	ΔE_b^{CP}	Complex	ΔE_b	E_{BSSE}^{CP}	ΔE_b^{CP}
Benzene (**B**)	**B-s-1**	1.92	0.75	1.17	**B-d-1**	3.87	1.52	2.35
					B-d-2	3.87	1.51	2.36
					B-d-3	3.16	1.15	2.01
Pyrene (**P**)	**P-s-1**	3.04	0.71	2.33	**P-d-1**	6.04	1.80	4.24
					P-d-2	5.75	1.81	3.94
					P-d-3	5.12	1.60	3.52
Coronene (**C**)	**C-s-1**	2.97	0.86	2.11	**C-d-1**	5.93	1.73	4.20
					C-d-2	6.17	1.82	4.35
Small graphene (**G1**)	**G1-s-1**	2.87	0.80	2.07	**G1-d-1**	5.69	1.60	4.09
	G1-s-2	2.95	0.85	2.10	**G1-d-2**	5.84	1.70	4.14
					G1-d-3	5.82	1.66	4.16
					G1-d-4	5.76	1.66	4.10
					G1-d-5	5.70	1.60	4.10
					G1-d-6	5.90	1.70	4.20
					G1-d-7	5.88	1.67	4.21
					G1-d-8	5.82	1.66	4.16
					G1-d-9	6.38	1.77	4.61
					G1-d-10	5.91	1.71	4.20
					G1-d-11	5.87	1.66	4.21
					G1-d-12	5.82	1.67	4.15
Large graphene (**G2**)	**G2-s-1**	2.84	0.72	2.12	**G2-d-1**	5.63	1.38	4.25
	G2-s-2	2.84	0.77	2.07	**G2-d-2**	5.69	1.56	4.13
	G2-s-3	2.96	0.85	2.11	**G2-d-3**	5.67	1.55	4.12
					G2-d-4	6.36	1.72	4.64
					G2-d-5	5.88	1.68	4.20
					G2-d-6	5.67	1.49	4.18
					G2-d-7	5.67	1.54	4.13
					G2-d-8	5.88	1.68	4.20

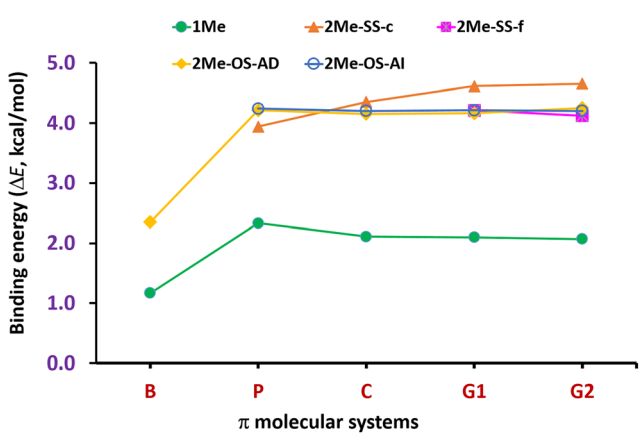

Fig. 6 Variation in BSSE-corrected binding energies for the most stable configurations of single and double methane binding with aromatic π-systems. **Me**, **SS-c**, **SS-f**, **OS**, **AD**, and **AI** stand for methane, same side-close, same side-far, opposite side, aligned directly, and aligned indirectly, respectively

d-2 and **P-d-2**, respectively. The rough estimate of the contribution of intermolecular H···H interactions in binding energy could be calculated by comparing two complexes, e.g., **P-d-2** and **P-d-3**. This pair is chosen because two methane molecules use the same set of six-membered rings, but they interact from same and opposite sides of the molecular plane in **P-d-2** and **P-d-3**, respectively. The similar pairs of complexes for other systems are **C-d-2** and **S_C-d-31** (see supplementary information, Fig. S6), **G1-d-9** and **G1-d-5**, and **G2-d-4** and **G2-d-2**. This comparison provides the rough estimate of (stabilizing) intermolecular H···H interactions of 0.42, 0.52, 0.51, and 0.51 kcal/mol contributed to the binding energies calculated for **P-d-2**, **C-d-2**, **G1-d-9**, and **G2-d-4**, respectively. It should be highlighted that BSSE-corrected binding energy for self-assembly of two methane molecules possessing H···H interactions is 0.47 kcal/mol (0.70 kcal/mol without BSSE correction) (Fig. 1). Our study reveals that the large surface area of graphene provides opportunity for multiple

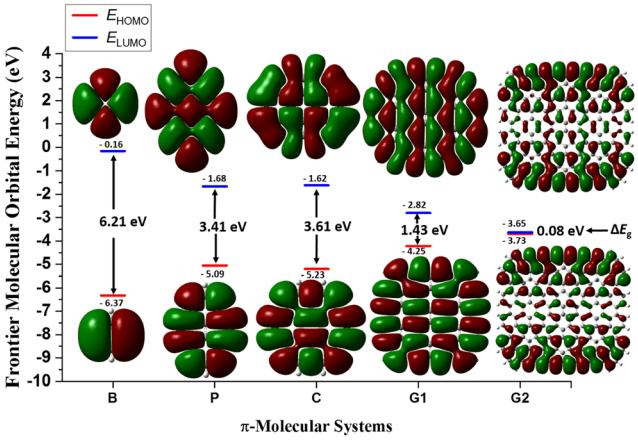

Fig. 7 Variation of HOMO and LUMO energies, and HOMO-LUMO energy gaps by increasing the size of π-molecular systems starting from benzene (**B**), pyrene (**P**), coronene (**C**), small graphene (**G1**) to large graphene (**G2**). The values and images of HOMO and LUMO were obtained at TPSSh/6-31G(d)//M06-2X/6-31G(d) level

C-H···π interactions with simultaneous H···H interactions among methane molecules when they adsorb on the surface. The binding of multiple methane molecules with graphene and modified graphene is under investigation in our lab to further understand the intermolecular H···H interactions and the potential of graphene-based systems as methane storage medium.

Figure 7 shows an almost zero value (0.08 eV) of HOMO-LUMO energy gap for large graphene model (**G2**). This value is in close agreement with experimental result for pristine graphene, which is well-known as a zero-band gap material. However, the small graphene (**G1**) yields a sizable value (1.43 eV) for HOMO-LUMO gap. Interestingly, the binding energy values are not noticeably different between **G1** and **G2** systems. HOMO and LUMO orbitals show an uneven distribution of orbitals with high concentration on the zigzag edges in large graphene while smaller π-systems including small graphene exhibit evenly distributed orbitals. Thus, the model

Table 3 Energies of HOMO (E_{HOMO}) and LUMO (E_{LUMO}), and HOMO-LUMO energy gap (E_g) in electron-volts (eV) for complexes of single and double methane binding with π-systems at TPSSh/6-31G(d)//M06-2X/6-31G(d) level

System	Single methane				Double methane			
	Complex	E_{HOMO}	E_{LUMO}	E_g	Complex	E_{HOMO}	E_{LUMO}	E_g
Benzene (**B**)	**B-s-1**	− 6.41	− 0.21	6.20	**B-d-1**	− 6.45	− 0.26	6.19
					B-d-2	− 6.44	− 0.25	6.19
					B-d-3	− 6.49	− 0.27	6.22
Pyrene (**P**)	**P-s-1**	− 5.11	− 1.69	3.42	**P-d-1**	− 5.14	− 1.72	3.42
					P-d-2	− 5.13	− 1.72	3.41
					P-d-3	− 5.13	− 1.71	3.42
Coronene (**C**)	**C-s-1**	− 5.24	− 1.63	3.61	**C-d-1**	− 5.26	− 1.64	3.62
					C-d-2	− 5.26	− 1.64	3.62
Small graphene (**G1**)	**G1-s-1**	− 4.26	− 2.83	1.43	**G1-d-1**	− 4.26	− 2.83	1.43
	G1-s-2	− 4.26	− 2.83	1.43	**G1-d-2**	− 4.27	− 2.84	1.43
					G1-d-3	− 4.27	− 2.84	1.43
					G1-d-4	− 4.26	− 2.83	1.43
					G1-d-5	− 4.26	− 2.83	1.43
					G1-d-6	− 4.27	− 2.84	1.43
					G1-d-7	− 4.24	− 2.84	1.40
					G1-d-8	− 4.26	− 2.83	1.43
					G1-d-9	− 4.26	− 2.81	1.45
					G1-d-10	− 4.27	− 2.84	1.43
					G1-d-11	− 4.27	− 2.84	1.43
					G1-d-12	− 4.26	− 2.81	1.45
Large graphene (**G2**)	**G2-s-1**	− 3.73	− 3.65	0.08	**G2-d-1**	− 3.74	− 3.66	0.08
	G2-s-2	− 3.73	− 3.65	0.08	**G2-d-2**	− 3.74	− 3.66	0.08
	G2-s-3	− 3.74	− 3.66	0.08	**G2-d-3**	− 3.74	− 3.66	0.08
					G2-d-4	− 3.74	− 3.66	0.08
					G2-d-5	− 3.74	− 3.66	0.08
					G2-d-6	− 3.74	− 3.66	0.08
					G2-d-7	− 3.74	− 3.66	0.08
					G2-d-8	− 3.74	− 3.66	0.08

Table 4 Scaled C-H stretching frequencies ($\nu_{C\text{-}H}$ in cm^{-1}) with corresponding intensities (Int. in km/mol) of free and adsorbed methane in the complexes obtained at M06-2X/6-31G (d) level

Symmetric stretching (interacting C-H)			Asymmetric stretching (interacting^i and non-interacting^n)					
System	$1\nu_1$ (Int.)	$2\nu_1$ (Int.)	$1\nu_3$ (Int.)	$2\nu_3$ (Int.)	$3\nu_3$ (Int.)	$4\nu_3$ (Int.)	$5\nu_3$ (Int.)	$6\nu_3$ (Int.)
CH_4	2928 (0)		3042 (21)	3042 (21)	3042 (21)			
B-s-1	2923 (1.4)		3035^n (26)	3038^n (17)	3042^i (10)			
B-d-1	2923 (2.8)	2923 (0)	3035^n (49)	3035^n (3.4)	3037^n (19)	3037^n (16)	3041^i (13)	3041^i (7.5)
B-d-2	2923 (0.6)	2923 (2.1)	3035^n (49)	3035^n (4)	3037^n (21)	3037^n (12)	3041^i (21)	3041^i (0)
B-d-3	2925 (0)	2925 (8.2)	3036^n (0)	3036^n (0)	3036^n (36)	3036^n (36)	3051^i (0)	3051^i (11)
P-s-1	2915 (0.7)		3028^i (11)	3028^i (10)	3032^n (33)			
P-d-1	2915 (1.1)	2916 (0.1)	3028^i (19)	3028^i (2.7)	3029^i (12)	3029^i (8)	3032^n (66)	3033^n (2.2)
P-d-2	2916 (0.9)	2917 (0)	3028^i (3.0)	3029^i (21)	3030^i (26)	3032^i (3)	3032^n (1.2)	3034^n (47)
P-d-3	2919 (1)	2919 (0)	3032^i (21)	3032^i (0)	3033^i (41)	3033^i (0)	3035^n (45)	3035^n (0)
C-s-1	2915 (0.5)		3028^i (9.2)	3029^i (9.6)	3033^n (33)			
C-d-1	2915 (0.5)	2916 (0.3)	3028^i (3)	3028^i (15)	3029^i (19)	3029^i (0)	3033^n (48)	3033^n (20)
C-d-2	2913 (0.4)	2916 (0.2)	3025^i (9.5)	3028^i (16)	3028^i (13)	3031^i (12)	3032^n (13)	3034^n (35)
G1-s-1	2916 (0.1)		3028^i (5.7)	3028^i (6.5)	3035^n (30)			
G1-s-2	2915 (0.3)		3027^i (6.8)	3028^i (8.7)	3034^n (35)			
G1-d-1	2915 (0.1)	2916 (0)	3028^i (0)	3028^i (12)	3028^i (13)	3028^i (0)	3035^n (0.2)	3035^n (62)
G1-d-2	2915 (0.4)	2915 (0.1)	3027^i (0)	3028^i (14)	3029^i (0.1)	3029^i (16)	3034^n (12)	3034^n (63)
G1-d-3	2915 (0.3)	2916 (0)	3027^i (0)	3027^i (13)	3029^i (12)	3029^i (0.3)	3034^n (9)	3035^n (62)
G1-d-4	2916 (0.3)	2916 (0)	3028^i (0)	3028^i (15)	3028^i (14)	3029^i (0)	3034^n (63)	3035^n (8.2)
G1-d-5	2916 (0.2)	2916 (0)	3028^i (13)	3028^i (0)	3028^i (0)	3028^i (12)	3035^n (62)	3035^n (0)
G1-d-6	2915 (0.7)	2915 (0)	3027^i (0)	3027^i (14)	3028^i (0)	3028^i (17)	3034^n (72)	3034^n (0.0)
G1-d-7	2915 (0.4)	2915 (0)	3027^i (0.1)	3027^i (12)	3028^i (1.1)	3028^i (11)	3034^n (64)	3034^n (5.3)
G1-d-8	2916 (0.0)	2916 (0.4)	3028^i (4.4)	3028^i (8.5)	3028^i (8.4)	3028^i (7.2)	3034^n (68)	3034^n (1.0)
G1-d-9	2913 (0.1)	2914 (0.0)	3024^i (0.7)	3025^i (15)	3026^i (12)	3028^i (0.1)	3033^n (0.6)	3035^n (54)
G1-d-10	2915 (0.5)	2915 (0.2)	3027^i (0.1)	3027^i (13)	3028^i (0)	3028^i (16)	3034^n (12)	3034^n (60)
G1-d-11	2915 (0.3)	2916 (0.2)	3027^i (0)	3027^i (12)	3028^i (15)	3028^i (0)	3035^n (9)	3035^n (60)
G1-d-12	2915 (0.4)	2916 (0.1)	3028^i (0.1)	3028^i (15)	3028^i (14)	3028^i (0)	3035^n (7.7)	3035^n (60)

Scaling factor of 0.947 was used based on ref. [67]. The intensities are given in parentheses. Interacting and non-interacting asymmetric C-H stretching of adsorbed methane molecule(s) are assigned by superscript "i" and "n" respectively

graphene **G2** could be suitable for future quantum mechanical studies for adsorption of small molecules and to predict electronic properties. Figure 7 shows a significant decrease of HOMO-LUMO gap from benzene (6.21 eV) to large graphene (0.08 eV).

It is known that the band gap of graphene must be opened to become useful in electronic circuits [76]. Using improved growth methods, the first graphene layer grown on the SiC(0001) surface has shown the semiconducting nature with a band gap greater than 0.5 eV. The specific substrate interactions with graphene lead to opening of band gap [77]. As shown the data in Fig. 7 and Table 3, HOMO and LUMO energy values, and HOMO-LUMO gaps are not significantly affected by binding of single and double methane molecule(s) with the PAHs and graphene. Pristine graphene systems interacting with small molecules that include α-amino acids reported similar findings [40–42, 78]. Recent experimental study showed that hybrid graphene (graphene with conductive polymer) material significantly enhanced photodetection via nanowire self-assembly in part by improving charge transport and charge transfer [79]. Similar kinds of hybrid materials have recently been reported in methane molecular sensing applications [80]. Thus, the results of pristine graphene will serve as a reference for future studies involving modified graphene-based materials including hybrid materials for methane storage and sensor applications.

C-H stretching frequencies

Experimental infrared (IR) spectra in gas phase were reported for methane-benzene and benzene dimer complexes [32, 81]. Furthermore, the adsorption of methane

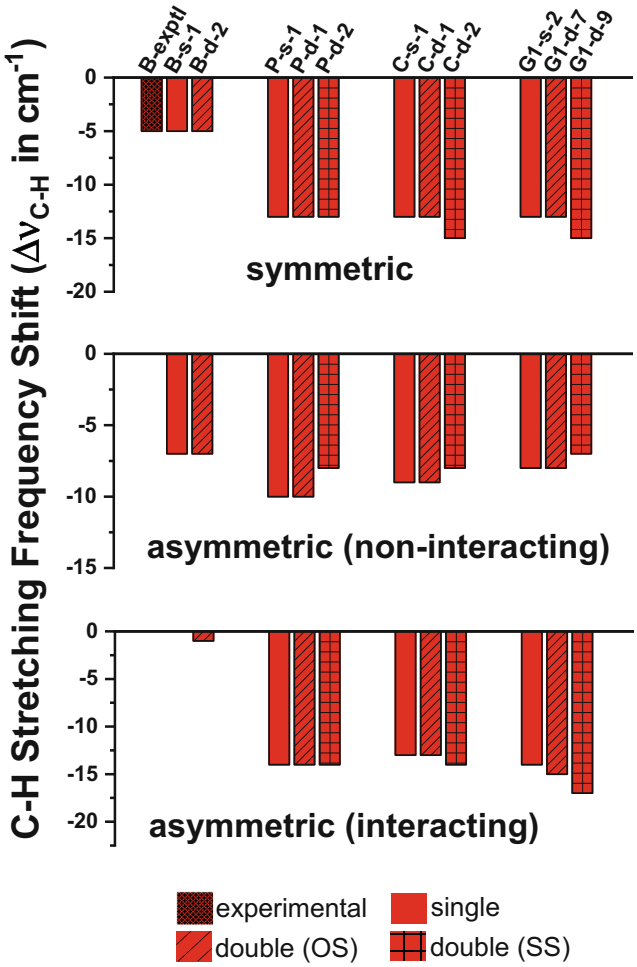

Fig. 8 C-H stretching frequency shifts obtained at M06-2X/6-31G(d) level for the most stable complexes of methane molecule(s) adsorbed on benzene (**B**), pyrene (**P**), coronene (**C**), and small graphene (**G1**). Frequencies with the highest intensities were selected in case of more than one frequency value. The letters **s** and **d** indicate the complexes having single and double methane, respectively. In the legend at the bottom, **SS** and **OS** correspondingly stand for the same side and opposite side when two methane molecules bind with π-systems. Experimental value of symmetric C-H stretching frequency shift was taken from ref. [39]

on single-wall carbon nanohorns (SWCNH) was characterized using IR spectroscopy [82]. The values of vibrational frequency shifts have been of interest for experimentalists and computational chemists [32, 81, 83–87]. C-H stretching frequency shift is calculated as the deviation of the value of C-H stretching frequency of methane in the complex with respect to the corresponding value in the free methane. Negative values of frequency shifts are called red shifts whereas positive values are called blue shifts. Computational studies reproduced the experimental values of very small red shifts of C-H stretching frequencies reported for methane-benzene and benzene dimer complexes [32, 36, 81, 83, 88]. Thus, computational results of vibrational frequency shifts of C-H stretching for the complexes of methane binding with π-systems including graphene will be useful for future experimental comparisons.

Frequency calculations were performed for the complexes shown in Figs. 2 and 3. Due to limited computational resources, it was not possible to complete the vibrational frequency calculations for large graphene (**G2**) and its complexes. For bare methane and complexes, symmetric and asymmetric C-H stretching frequency (scaled) values along with intensities are listed in Table 4. Generally, the C-H stretching frequencies of CH_4 in the complexes are red-shifted with respect to bare methane. Symmetric stretching frequencies are lower magnitudes than asymmetric stretching frequencies. Among the π-systems, benzene complexes exhibit higher values than the complexes of **P**, **C**, and **G1**. Small changes in frequencies are observed when we move from pyrene to coronene complexes. Again, one cannot notice large changes in frequency values from coronene to small graphene complexes. Vibrational frequencies are not helpful in distinguishing different complexes of double methane with small graphene (**G1**).

Figure 8 depicts the selected C-H stretching frequency shifts of the important complexes of all π-systems and the available experimental frequency shift for methane-benzene complex for comparison purpose. Symmetric stretching frequency of interacting C-H bond of methane is red-shifted to 5 cm^{-1} in case of **B-s-1** and **B-d-2** complexes, and this value matches with the experimental data. Previous theoretical studies did not reproduce the experimental symmetric stretching frequency shift of C-H bond for methane-benzene complex most likely due to less fine grid used in earlier studies [36, 39, 82]. Symmetric and interacting asymmetric red shifts are marginally larger for two methane molecules close to each other on the same side of **C** and **G1** compared to single methane molecule as well as two methane molecules on the opposite sides of the plane of **C** and **G1**. Conversely, the red shifts of non-interacting asymmetric C-H stretching frequencies are slightly diminished for complexes of two methane molecules self-interacting as well as binding with the π-systems of **P**, **C**, and **G1**. Furthermore, calculations for methane dimer complex without the presence of any π-surface resulted in red shift values of 2 to 3 cm^{-1}. This explains the differences of frequency shifts observed between the complexes possessing two methane molecules on same and opposite sides of π-planes in case of **C** and **G1**. This study provides knowledge on the effect of simultaneous methane addition to the varying sizes of π-systems. Importantly, the existence and role of intermolecular CH···HC interactions between two methane in the complexes possessing C-H···π interactions are revealed. Computational explorations could be helpful in

designing and realization of graphene (**G**)-based nanosystems for methane (CH_4) storage and sensors.

Conclusions

Density functional theory at M06-2X/6-31G(d) level calculations were performed to understand the binding of single and double methane molecule(s) with graphene and other π-systems of benzene, pyrene, and coronene. In this study, various isoenergetic structures were encountered for the complexes between methane and polycyclic π-systems. Significant increase in binding affinity of methane is observed while moving from benzene to other planar molecules considered here. Methane molecule prefers three C-H···π interactions when it binds with all polycyclic π-systems. The binding energies obtained for coronene and graphene are similar. Increasing the number of methane molecules from one to two increases the binding energy by almost the factor of 2 for all π-systems considered. Our results reveal that intermolecular CH···HC interactions between two methane molecules have shown an impact on binding energies while those molecules simultaneously interact with graphene or coronene. Though H···H contacts are weak interactions, a buildup can result in a significantly sticky interactions. To fully understand the nature of "sticky" H···H interactions, it is important to consider their role in contributing to overall binding. The preference of same or opposite side is irrelevant if two methane molecules do not interact with each other.

Complex structures and binding energies reveal that the edge rings have negligible effect compared to inner rings of graphene for methane binding. HOMO-LUMO energy gaps are not significantly affected by binding of single and double methane molecule(s) with the π-systems. Large graphene model (**G2**) yields almost zero value (0.08 eV) of HOMO-LUMO energy gap that is closer to experimental result for pristine graphene (zero band gap) whereas the small graphene (**G1**) provides the value of 1.43 eV. The binding energy values are not noticeably different between **G1** and **G2** systems. C-H stretching frequency of methane is red-shifted when it is in the complexes. Computational results of vibrational frequency shifts of C-H stretching for the complexes of methane binding with graphene and other π-systems will be useful for future experimental comparisons. Our study reveals that the large surface area of graphene provides opportunity for multiple C-H···π interactions along with stabilizing H···H interactions between two methane molecules adsorbing on the surface. Both sides of graphene sheet can be utilized by engineers when considering development of efficient storage systems. Computational data and knowledge provide insights in effective designing and realization of graphene (**G**)-based nanomaterials for methane (CH_4) storage and sensors.

Funding TD recognizes the National Science Foundation (NSF) for the grants through HBCU-UP RIA (Grant Number: 1601071), HBCU-UP TIP (Grant Number: 1623287), and RISE (Grant Number: 1924204). Graduate Studies Office at Clark Atlanta University is thanked for the graduate student support to JL through Title III program. DD acknowledges Saudi Arabian Cultural Mission (SACM) for the scholarship. Extreme Science and Engineering Discovery Environment (XSEDE) is acknowledged for the computational resources (resource allocation grant DMR 160170).

Compliance with ethical standards

Conflict of interest The authors declare that there are no conflicts of interest.

References

1. Bowers GM, Loring JS, Schaef HT, Walter ED, Burton SD, Hoyt DW, Cunniff SS, Loganathan N, Kirkpatrick RJ (2018) Interaction of hydrocarbons with clays under reservoir conditions: in situ infrared and nuclear magnetic resonance spectroscopy and X-ray diffraction for expandable clays with variably wet supercritical methane. ACS Earth Space Chem 2:640–652
2. Li W, Liu Y, Xiao S, Zhang Y, Chai L (2018) An investigation of the underlying evolution of shale gas research's domain based on the co-word network. Sustainability 10:164
3. Wang Q, Chen X, Jha AN, Rogers H (2014) Natural gas from shale formation—the evolution, evidences and challenges of shale gas revolution in United States. Renew Sust Energ Rev 30:1–28
4. Wang F, Liu G-Q, Meng H-L, Guo G, Luo S-J, Guo R-B (2016) Improved methane hydrate formation and dissociation with nanosphere-based fixed surfactants as promoters. ACS Sustain Chem Eng 4:2107–2113
5. Collett T, Bahk J-J, Baker R, Boswell R, Divins D, Frye M, Goldberg D, Husebø J, Koh C, Malone M, Morell M, Myers G, Shipp C, Torres M (2015) Methane hydrates in nature—current knowledge and challenges. J Chem Eng Data 60:319–332
6. Jiao Y, Wang L, Zhang L, An W, Wang W, Zhou W, Tadé MO, Shao Z, Bai J, Li S-D (2018) Direct operation of solid oxide fuel cells on low-concentration oxygen-bearing coal-bed methane with high stability. Energy Fuel 32:4547–4558
7. Karacan COR, Ruiz FA, Cotè M, Phipps S (2011) Coal mine methane; a review of capture and utilization practices with benefits to mining safety and to greenhouse gas reduction. Int J Coal Geol 86: 121–156
8. Zhou Y, Fu Q, Shen Y, Sun W, Zhang D, Li D, Yan H (2016) Upgrade of low-concentration oxygen-bearing coal bed methane by a vacuum pressure swing adsorption process: performance study and safety analysis. Energy Fuel 30:1496–1509
9. Vielstädte L, Haeckel M, Karstens J, Linke P, Schmidt M, Steinle L, Wallmann K (2017) Shallow gas migration along hydrocarbon wells—an unconsidered, anthropogenic source of biogenic methane in the North Sea. Environ Sci Technol 51:10262–10268
10. Chen JJ, Li WW, Li XL, Yu HQ (2012) Improving biogas separation and methane storage with multilayer graphene nanostructure via layer spacing optimization and lithium doping: a molecular simulation investigation. Environ Sci Technol 46:10341–10348
11. Dhingra R, Christensen ER, Liu Y, Zhong BO, Wu C-F, Yost MG, Remais JV (2011) Greenhouse gas emission reductions from domestic anaerobic digesters linked with sustainable sanitation in rural China. Environ Sci Technol 45:2345–2352
12. Lee H-H, Ahn S-H, Nam B-U, Kim B-S, Lee G-W, Moon D, Shin HJ, Han KW, Yoon J-H (2012) Thermodynamic stability,

spectroscopic identification, and gas storage capacity of CO_2–CH_4–N_2 mixture gas hydrates: implications for landfill gas hydrates. Environ Sci Technol 46:4184–4190
13. Zhang X, Sun Y, Su W, Wang X (2016) Adsorption equilibria of C1–C4 from natural gas on graphene sheets. J Chem Eng Data 61: 1667–1675
14. Zhu ZW, Zheng QR (2016) Methane adsorption on the graphene sheets, activated carbon and carbon black. Appl Therm Eng 108(Supplement C):605–613
15. Chouhan RK, Ulman K, Narasimhan S (2015) Graphene oxide as an optimal candidate material for methane storage. J Chem Phys 143:044704
16. Mahmoudian L, Rashidi A, Dehghani H, Rahighi R (2016) Single-step scalable synthesis of three-dimensional highly porous graphene with favorable methane adsorption. Chem Eng J 304(Supplement C):784–792
17. Patel P (2017) Chemical sensing: looking for methane leaks. C&EN Global Enterprise 95:19–22
18. Patel P (2017) Monitoring methane. ACS Cent Sci 3:679–682
19. Yang N, Yang D, Zhang G, Chen L, Liu D, Cai M, Fan X (2018) The effects of graphene stacking on the performance of methane sensor: a first-principles study on the adsorption, band gap and doping of graphene. Sensors (Basel, Switzerland) 18:422
20. Srinivas G, Guo ZX (2015) Graphene-based materials: synthesis and gas sorption, storage and separation. Prog Mater Sci 69:1–60
21. García-Hernández E, Salazar-García E, Shakerzadeh E, Chigo-Anotac E (2020) Effect of dehydrogenated hydrocarbon doping on the electronic properties of graphene-type nanosheets. Phys Lett A 384:126702
22. Chigo-Anota E, Alejandro MA, Hernández AB, Torres JJS, Castro M (2016) Long range corrected-wPBE based analysis of the H_2O adsorption on magnetic BC_3 nanosheets. RSC Adv 6:20409–20421
23. Hernández JMG, Anota EC, de la Cruz MRT, Melchor MG, Gregorio Hernández Cocoletzi GH (2012) First principles studies of the graphene-phenol interactions. J Mol Model 18:3857–3866
24. Dinadayalane T, Leszczynska D, Leszczynski J (2012) Graphene: properties, biomedical applications and toxicity. In: Puzyn T, Leszczynski J (eds) Towards efficient designing of safe nanomaterials: innovative merge of computational approaches and experimental techniques, vol 25. Royal Society of Chemistry, Cambridge, pp 1–26
25. Dinadayalane TC, Leszczynski J (2016) Fundamental structural, electronic, and chemical properties of carbon nanostructures: graphene, fullerenes, carbon nanotubes, and their derivatives. In: Leszczynski J (ed) Handbook of computational chemistry. Springer, Dordrecht, pp 1–84
26. Feng S, dos Santos MC, Carvalho BR, Lv R, Li Q, Fujisawa K, Elías AL, Lei Y, Perea-López N, Endo M, Pan M, Pimenta MA, Terrones M (2016) Ultrasensitive molecular sensor using N-doped graphene through enhanced Raman scattering. Sci Adv 2:e1600322
27. Wu Z, Chen X, Zhu S, Zhou Z, Yao Y, Quan W, Liu B (2013) Room temperature methane sensor based on graphene nanosheets/polyaniline nanocomposite thin film. IEEE Sensors J 13:777–782
28. Pykal M, Jurečka P, Karlický F, Otyepka M (2016) Modelling of graphene functionalization. Phys Chem Chem Phys 18:6351–6372
29. Tsuzuki S, Honda K, Uchimaru T, Mikami M, Tanabe K (2000) The magnitude of the CH/π interaction between benzene and some model hydrocarbons. J Am Chem Soc 122:3746–3753
30. Ramezanpour M, Leung SSW, Delgado-Magnero KH, Bashe BYM, Thewalt J, Tieleman DP (2016) Computational and experimental approaches for investigating nanoparticle-based drug delivery systems. Biochim Biophys Acta Biomembr 1858:1688–1709
31. Ringer AL, Figgs MS, Sinnokrot MO, Sherrill CD (2006) Aliphatic C−H/π interactions: methane−benzene, methane−phenol, and methane−indole complexes. J Phys Chem A 110:10822–10828
32. Shibasaki K, Fujii A, Mikami N, Tsuzuki S (2006) Magnitude of the CH/π interaction in the gas phase: experimental and theoretical determination of the accurate interaction energy in benzene-methane. J Phys Chem A 110:4397–4404
33. Tsuzuki S, Honda K, Fujii A, Uchimaru T, Mikami M (2008) CH/π interactions in methane clusters with polycyclic aromatic hydrocarbons. Phys Chem Chem Phys 10:2860–2865
34. Karthikeyan S, Ramanathan V, Mishra BK (2013) Influence of the substituents on the CH···π interaction: benzene-methane complex. J Phys Chem A 117:6687–6694
35. Smith DGA, Patkowski K (2013) Interactions between methane and polycyclic aromatic hydrocarbons: a high accuracy benchmark study. J Chem Theory Comput 9:370–389
36. Paytakov G, Dinadayalane T, Leszczynski J (2015) Toward selection of efficient density functionals for van der Waals molecular complexes: comparative study of C–H···π and N–H···π interactions. J Phys Chem A 119:1190–1200
37. Vekeman J, G. Cuesta I, Faginas-Lago N, Wilson J, Sánchez-Marín J, Sánchez de Merás A (2018) Potential models for the simulation of methane adsorption on graphene: development and CCSD(T) benchmarks. Phys Chem Chem Phys 20:25518–25530
38. Qiu N-X, Xue Y, Guo Y, Sun W-J, Chu W (2012) Adsorption of methane on carbon models of coal surface studied by the density functional theory including dispersion correction (DFT-D3). Comput Theor Chem 992:37–47
39. Morita S-i, Fujii A, Mikami N, Tsuzuki S (2006) Origin of the attraction in aliphatic C−H/π interactions: infrared spectroscopic and theoretical characterization of gas-phase clusters of aromatics with methane. J Phys Chem A 110:10583–10590
40. Daggag D, Lazare J, Dinadayalane T (2019) Conformation dependence of tyrosine binding on the surface of graphene: bent prefers over parallel orientation. Appl Surf Sci 483:178–186
41. Daggag D, Dorlus T, Dinadayalane T (2019) Binding of histidine and proline with graphene: DFT study. Chem Phys Lett 730:147–152
42. Daggag D, Lazare J, Dinadayalane T (2019) Data related to conformation dependence of tyrosine binding on the surface of graphene: bent prefers over parallel orientation. Data Brief 26: 104420
43. Pandit S, De M (2017) Interaction of amino acids and graphene oxide: trends in thermodynamic properties. J Phys Chem C 121: 600–608
44. Vovusha H, Sanyal S, Sanyal B (2013) Interaction of nucleobases and aromatic amino acids with graphene oxide and graphene flakes. J Phys Chem Lett 4:3710–3718
45. Nassef HM, Hagar M, Malek Z, Othman AM (2018) Uptake of tyrosine amino acid on nano-graphene oxide. Materials 11:68
46. Plevin MJ, Bryce DL, Boisbouvier J (2010) Direct detection of CH/π interactions in proteins. Nat Chem 2:466
47. Jenness GR, Karalti O, Jordan KD (2010) Benchmark calculations of water–acene interaction energies: extrapolation to the water–graphene limit and assessment of dispersion–corrected DFT methods. Phys Chem Chem Phys 12:6375–6381
48. Rubeš M, Bludský O (2009) DFT/CCSD(T) investigation of the interaction of molecular hydrogen with carbon nanostructures. ChemPhysChem 10:1868–1873
49. Rubeš M, Nachtigall P, Vondrášek J, Bludský O (2009) Structure and stability of the water−graphite complexes. J Phys Chem C 113: 8412–8419
50. Lazar P, Karlický F, Jurečka P, Kocman M, Otyepková E, Šafářová K, Otyepka M (2013) Adsorption of small organic molecules on graphene. J Am Chem Soc 135:6372–6377
51. Podeszwa R (2010) Interactions of graphene sheets deduced from properties of polycyclic aromatic hydrocarbons. J Chem Phys 132: 044704

52. Medeiros PVC, Gueorguiev GK, Stafström S (2015) Bonding, charge rearrangement and interface dipoles of benzene, graphene, and PAH molecules on Au(111) and Cu(111). Carbon 81:620–628
53. Vidali G, Ihm G, Kim H-Y, Cole MW (1991) Potentials of physical adsorption. Surf Sci Rep 12:135–181
54. Do DD, Do HD (2005) Evaluation of 1-site and 5-site models of methane on its adsorption on graphite and in graphitic slit pores. J Phys Chem B 109:19288–19295
55. Albesa AG, Llanos JL, Vicente JL (2008) Comparative study of methane adsorption on graphite. Langmuir 24:3836–3840
56. Valiev M, Bylaska EJ, Govind N, Kowalski K, Straatsma TP, Van Dam HJJ, Wang D, Nieplocha J, Apra E, Windus TL, de Jong WA (2010) NWChem: a comprehensive and scalable open-source solution for large scale molecular simulations. Comput Phys Commun 181:1477–1489
57. Zhao Y, Truhlar DG (2008) The M06 suite of density functionals for main group thermochemistry, thermochemical kinetics, noncovalent interactions, excited states, and transition elements: two new functionals and systematic testing of four M06-class functionals and 12 other functionals. Theor Chem Accounts 120:215–241
58. Gao T, Li H, Li W, Li L, Fang C, Li H, Hu L, Lu Y, Su Z-M (2016) A machine learning correction for DFT non-covalent interactions based on the S22, S66 and X40 benchmark databases. J Cheminform 8:24
59. Boys SF, Bernardi F (1970) The calculation of small molecular interactions by the differences of separate total energies. Some procedures with reduced errors. Mol Phys 19:553–566
60. Tao J, Perdew JP, Staroverov VN, Scuseria GE (2003) Climbing the density functional ladder: nonempirical meta-generalized gradient approximation designed for molecules and solids. Phys Rev Lett 91:146401
61. Staroverov VN, Scuseria GE, Tao J, Perdew JP (2004) Erratum: "Comparative assessment of a new nonempirical density functional: molecules and hydrogen-bonded complexes" [J Chem Phys (2003) 119:12129]. J Chem Phys 121:11507–11507
62. Barone V, Hod O, Peralta JE, Scuseria GE (2011) Accurate prediction of the electronic properties of low-dimensional graphene derivatives using a screened hybrid density functional. Acc Chem Res 44:269–279
63. Dinadayalane TC, Leszczynski J (2013) Comparative theoretical study on the positional preference for functionalization of two OH and SH groups with (5,5) armchair SWCNT. J Phys Chem C 117: 14441–14450
64. Herath D, Dinadayalane T (2017) Computational investigation of double nitrogen doping on graphene. J Mol Model 24:26
65. Wróbel J, Kurzydłowski KJ, Hummer K, Kresse G, Piechota J (2009) Calculations of ZnO properties using the Heyd-Scuseria-Ernzerhof screened hybrid density functional. Phys Rev B 80: 155124
66. Wu J, Hagelberg F, Dinadayalane TC, Leszczynska D, Leszczynski J (2011) Do Stone–Wales defects alter the magnetic and transport properties of single-walled carbon nanotubes? J Phys Chem C 115: 22232–22241
67. NIST Computational Chemistry Comparison and Benchmark Database (2019) National Institute of Standards and Technology (NIST). http://cccbdb.nist.gov.
68. Rayment T, Thomas RK, Bomchil G, White JW (1981) The structure and properties of methane adsorbed on graphitized carbon black determined by neutron diffraction. Mol Phys 43:601–620
69. Danovich D, Shaik S, Neese F, Echeverria J, Aullon G, Alvarez S (2013) Understanding the nature of the CH···HC interactions in alkanes. J Chem Theory Comput 9:1977–1991
70. Wang C, Mo Y, Wagner JP, Schreiner PR, Jemmis ED, Danovich D, Shaik S (2015) The self-association of graphane is driven by London dispersion and enhanced orbital interactions. J Chem Theory Comput 11:1621–1630
71. Rösel S, Quanz H, Logemann C, Becker J, Mossou E, Cañadillas-Delgado L, Caldeweyher E, Grimme S, Schreiner PR (2017) London dispersion enables the shortest intermolecular hydrocarbon H···H contact. J Am Chem Soc 139:7428–7431
72. Schreiner P, Chernish L, Gunchenko P, Tikhonchuk E, Hausmann H, Serafin M, Schlecht S, Dahl J, Carlson R, Fokin A (2011) Overcoming lability of extremely long alkane carbon-carbon bonds through dispersion forces. Nature 477:308–311
73. Grimme S, Schreiner PR (2011) Steric crowding can stabilize a labile molecule: solving the hexaphenylethane riddle. Angew Chem Int Ed 50:12639–12642
74. Fokin A, Gerbig D, Schreiner P (2011) σ/σ- and π/π-interactions are equally important: multilayered graphanes. J Am Chem Soc 133:20036–20039
75. Fokin AA, Chernish LV, Gunchenko PA, Tikhonchuk EY, Hausmann H, Serafin M, Dahl JEP, Carlson RMK, Schreiner PR (2012) Stable alkanes containing very long carbon–carbon bonds. J Am Chem Soc 134(33):13641–13650
76. Palacios T, Hsu A, Wang H (2010) Applications of graphene devices in RF communications. IEEE Commun Magaz 48:122–128
77. Nevius MS, Conrad M, Wang F, Celis A, Nair MN, Taleb-Ibrahimi A, Tejeda A, Conrad EH (2015) Semiconducting graphene from highly ordered substrate interactions. Phys Rev Lett 115:136802
78. Anithaa VS, Shankar R, Vijayakumar S (2017) DFT-based investigation on adsorption of methane on pristine and defected graphene. Struct Chem 28:1935–1952
79. Li M, Nykypanchuk D, Cotlet M (2018) Improving the responsivity of hybrid graphene–conductive polymer photodetectors via nanowire self-assembly. ACS Photon 5:4296–4302
80. Dosi M, Lau I, Zhuang Y, Simakov DSA, Fowler MW, Pope MA (2019) Ultrasensitive electrochemical methane sensors based on solid polymer electrolyte-infused laser-induced graphene. ACS Appl Mater Interfaces 11:6166–6173
81. Erlekam U, Frankowski M, Meijer G, von Helden G (2006) An experimental value for the B_{1u} C–H stretch mode in benzene. J Chem Phys 124:171101
82. Hashimoto S, Fujimori T, Tanaka H, Urita K, Ohba T, Kanoh H, Itoh T, Asai M, Sakamoto H, Niimura S, Endo M, Rodriguez-Reinoso F, Kaneko K (2011) Anomaly of CH_4 molecular assembly confined in single-wall carbon nanohorn spaces. J Am Chem Soc 133:2022–2024
83. Dinadayalane TC, Leszczynski J (2009) In the pursuit of small "red shift" of C–H stretching vibrational frequency of C–H···π interactions for benzene dimer: how to amend MP2 calculations to reproduce the experimental results. J Chem Phys 130:081101
84. Zhang G, Wang W, Chen D (2008) Chemical origin of blue and red shifts of C–H stretching vibrations in M^+–C_2H_2 (M=V, Fe, Co, Ni) and M^+–C_6H_6 (M=V, Si, Ni) complexes. Chem Phys 354:225–229
85. Hermida-Ramón JM, Graña AM (2007) Blue-shifting hydrogen bond in the benzene–benzene and benzene–naphthalene complexes. J Comput Chem 28:540–546
86. Dinadayalane TC, Paytakov G, Leszczynski J (2013) Computational study on C–H···π interactions of acetylene with benzene, 1,3,5-trifluorobenzene and coronene. J Mol Model 19: 2855–2864
87. Hobza P, Špirko V, Selzle HL, Schlag EW (1998) Anti-hydrogen bond in the benzene dimer and other carbon proton donor complexes. J Phys Chem A 102:2501–2504
88. Wang W, Pitoňák M, Hobza P (2007) C-H stretching vibrational shift of benzene dimer: consistency of experiment and calculation. ChemPhysChem 8:2107–2111